



NRC Publications Archive Archives des publications du CNRC

Nanostructured titania/hydroxyapatite composite coatings deposited by high velocity oxy-fuel (HVOF) spraying

Gaona, M.; Lima, R. S.; Marple, B. R.

This publication could be one of several versions: author's original, accepted manuscript or the publisher's version. /
La version de cette publication peut être l'une des suivantes : la version prépublication de l'auteur, la version
acceptée du manuscrit ou la version de l'éditeur.

For the publisher's version, please access the DOI link below. / Pour consulter la version de l'éditeur, utilisez le lien
DOI ci-dessous.

Publisher's version / Version de l'éditeur:

<https://doi.org/10.1016/j.msea.2006.12.090>

Materials science and engineering A, 458, 1-2, pp. 141-149, 2007-01-03

NRC Publications Record / Notice d'Archives des publications de CNRC:

<https://nrc-publications.canada.ca/eng/view/object/?id=25bd2235-175c-4d39-87a4-0d8d5bd526c8>

<https://publications-cnrc.canada.ca/fra/voir/objet/?id=25bd2235-175c-4d39-87a4-0d8d5bd526c8>

Access and use of this website and the material on it are subject to the Terms and Conditions set forth at

<https://nrc-publications.canada.ca/eng/copyright>

READ THESE TERMS AND CONDITIONS CAREFULLY BEFORE USING THIS WEBSITE.

L'accès à ce site Web et l'utilisation de son contenu sont assujettis aux conditions présentées dans le site

<https://publications-cnrc.canada.ca/fra/droits>

LISEZ CES CONDITIONS ATTENTIVEMENT AVANT D'UTILISER CE SITE WEB.

Questions? Contact the NRC Publications Archive team at

PublicationsArchive-ArchivesPublications@nrc-cnrc.gc.ca. If you wish to email the authors directly, please see the
first page of the publication for their contact information.

Vous avez des questions? Nous pouvons vous aider. Pour communiquer directement avec un auteur, consultez la
première page de la revue dans laquelle son article a été publié afin de trouver ses coordonnées. Si vous n'arrivez
pas à les repérer, communiquez avec nous à PublicationsArchive-ArchivesPublications@nrc-cnrc.gc.ca.



Nanostructured titania/hydroxyapatite composite coatings deposited by high velocity oxy-fuel (HVOF) spraying

M. Gaona^a, R.S. Lima^{b,*}, B.R. Marple^b

^a Thermal Spray Centre, Universitat de Barcelona, Martí i Franquès 1, 08028 Barcelona, Spain

^b National Research Council of Canada, 75 de Mortagne Blvd., Boucherville, QC J4B 6Y4, Canada

Received 16 October 2006; received in revised form 8 December 2006; accepted 15 December 2006

Abstract

Pure nanostructured titania (TiO₂) and blends with 10 and 20 wt% hydroxyapatite (HA) powders were sprayed onto Ti–6Al–4V substrates using a high velocity oxy-fuel (HVOF) system. The feedstock powders employed in this work were engineered to exhibit similar particle size distributions in order to generate similar values of particle temperature and velocity in the spray jet. By achieving these characteristics it was assumed that the differences in coating properties and microstructures produced in this study were mainly related to the nature and composition of the feedstock powders, rather than to the spraying parameters or in-flight particle characteristics. The microstructure, porosity, roughness, Vickers hardness and bond strength (ASTM C633) of these coatings were analyzed and evaluated. X-ray diffraction (XRD) patterns showed that no detectable chemical reaction occurred between the nanostructured TiO₂ and HA phases during the spray process. Due to the poor mechanical performance of HA, its addition decreased the bond strength and hardness values of the coatings, especially when the content of HA was 20 wt%; however, the bond strength values were still much superior to those of HA thermally sprayed coatings. The addition of HA to nanostructured titania for producing HVOF-sprayed coatings could be very interesting for biomedical applications due to the combination of the good mechanical performance and chemical stability of nanostructured titania and a bioactive phase (HA) that can enhance the bio-performance of the coating.

Crown Copyright © 2007 Published by Elsevier B.V. All rights reserved.

Keywords: Thermal spray; High velocity oxy-fuel (HVOF); Nanostructured titania (TiO₂); Hydroxyapatite (HA); Titania-hydroxyapatite; Mechanical performance

1. Introduction

1.1. Hydroxyapatite thermal spray coatings

Hydroxyapatite (HA) has been extensively studied and clinically applied for its bioactive properties in medicine. HA is too brittle to be used as bulk material under loaded conditions, so HA is normally applied as a coating on metallic substrates in order to combine the mechanical strength of metals with the excellent biological properties of HA. Although HA coatings have been applied by a wide range of surface deposition techniques, the air plasma spray (APS) process is still the most commercially used technology and is a relatively efficient, fast and economic approach. During the spraying, the material is fully or partially melted in the plasma jet and sprayed at

high velocities onto a substrate to build up the coating. However, due to the extremely high temperatures of the plasma jet and the rapid cooling rate of sprayed particles when impacting the substrate, the degradation of HA to other bioresorbable phases, such as tricalcium phosphate (α or β -TCP), tetracalcium phosphate (TTCP) or the non-biocompatible CaO is inevitable [1,2].

It has been pointed out that the use of HA-coated implants is often based on relatively short-term medical data that may not necessarily be an indicator of the long-term performance. Some authors have reported that the effects of disintegration of the HA coatings only become clinically evident after 5–6 years in HA-coated acetabular prostheses and that dissolution is accelerated on areas subjected to a high level of loading [3]. Studies involving analysis of the HA coating surface after implantation indicated dissolution, osteoclastic resorption, and carbonate apatite precipitation had occurred [4,5]. These are among the reasons why new biocompatible coatings with improved mechanical strength, chemical stability in the human

* Corresponding author. Tel.: +1 450 641 5150; fax: +1 450 641 5105.
E-mail address: rogerio.lima@nrc-nrc.gc.ca (R.S. Lima).

body and even higher biocompatibility levels are being sought by various researchers.

1.2. Titania (TiO_2) as a biomedical coating

The use of titanium metal, considered to be bioinert, as an implant material is based on its load bearing properties and the good biocompatibility properties of its thin native oxide layer (TiO_2), which does not exhibit resorption by the human body fluids. These properties have led to titania being deposited onto metallic substrates for biomedical applications, although it is generally considered not as bioactive as HA.

It has been reported that high velocity oxy-fuel (HVOF) sprayed nanostructured titania coatings exhibit higher bond strength, higher crack propagation resistance and higher wear resistance compared to the conventional titania coatings [6,7]. It was hypothesized that the semi-molten nanostructured titania particles (nanozones), spread and embedded throughout the coating microstructure, were responsible for the good mechanical behavior, i.e., it was suggested that they acted as crack arresters, thereby improving coating toughness [6,7]. In addition to the good mechanical properties, the nanostructured titania coatings and bulk were shown to possess properties important for implantation; for example, a bonelike apatite formation on the surface of the coating after immersion in simulated body fluids, an osteoblast cell growth (in vitro) equivalent or superior to that of APS HA coatings, and an increase in osteoblast adhesion (cell cultures) compared to non-nanostructured materials [8–10]. It is believed that the nanostructured surface topography plays a significant role in the adsorption of ions and adhesion protein cells of the osteoblasts (vitronectin and fibronectin) [11,12].

HVOF-sprayed nanostructured TiO_2 coatings have demonstrated superior mechanical behaviour when compared to that of HA thermal spray coatings (APS or HVOF-sprayed) [13]. As previously stated, this type of TiO_2 coating exhibited an osteoblast cell growth (in vitro) equivalent or superior to that of APS HA coatings [9]. It is speculated that this “good” biological performance could be enhanced by the addition of HA in the coating composition.

The information available to the authors indicated that TiO_2 + HA mixtures have not been used in the production of implants on a commercial scale, however, it is possible to find different references in the literature about the use of TiO_2 + HA composites as biomedical materials. Li [14] produced TiO_2 and TiO_2 + 15 vol.% HA rods via hot isostatic pressing. These rods were implanted in the femurs of rabbits. After three months of implantation the rabbits were euthanized and push out tests were performed. The TiO_2 + 15 vol.% HA composite rods showed an increase of shear strength of 1.7 times when compared to that of the pure TiO_2 rods. Ramires et al. [15] studied the biocompatibility (in vitro) of TiO_2 + HA coatings prepared via sol-gel. The results demonstrated that the TiO_2 + HA coatings were not cytotoxic and allowed the proliferation of human osteoblast-like cells. The bioactivity of the TiO_2 + HA coatings was the result of the presence of hydroxyl groups detected on their surfaces, which promoted calcium and phosphate precipitation, improving the interactions with the osteoblast cells. These ref-

erences confirm that TiO_2 + HA mixtures have potential as biomaterials.

The objective of this work was to HVOF spray nanostructured TiO_2 , nanostructured TiO_2 + 10 wt% HA and nanostructured TiO_2 + 20 wt% HA feedstock powders, in order to engineer coatings having the good mechanical performance of the HVOF-sprayed nanostructured titania and the proven biocompatibility of HA. In order to try to separate the effects of powder composition and morphology on the microstructure and mechanical performance of the coatings from that of the in-flight characteristics of the particles during thermal spraying, the feedstock powders were engineered to exhibit a similar particle size distribution and were thermally sprayed by choosing spray parameters that produced similar values of particle temperature and velocity in the HVOF jet. Using this processing approach it was assumed that any differences in mechanical performance and microstructure observed among the three coatings would be mainly related to the composition/morphology of the powders, and not the in-flight particle characteristics, i.e., particle temperature and velocity.

2. Experimental procedure

2.1. Feedstock powders

The feedstock powder mixtures were composed of 80 wt% nano TiO_2 –20 wt% HA, 90 wt% nano TiO_2 –10 wt% HA and pure nanostructured titania. The starting nanostructured titania feedstock (VHP-DCS (5–20 μm), Altair Nanomaterials Inc., Reno, NV, USA) had a nominal particle size distribution from 5 to 22 μm . The HA powder (Captal 30 SD, Plasma Biotal, UK) was pure and highly crystalline and was sieved to produce particles with diameters smaller than 22 μm to ensure the uniformity of the mixture with titania. The feedstock powders were prepared through a mechanical-blending process in a planetary mill (P5, Fritsch GmbH, Germany). Powder particle size distribution was performed by a laser diffraction particle size analyzer (Beckman Coulter LS 13320, Beckman Coulter, Miami, FL, USA).

2.2. Thermal spraying and in-flight particle diagnostics

The three feedstock powders were thermally sprayed via the HVOF technique using an oxy-propylene based HVOF torch (Diamond Jet 2700-hybrid, Sulzer Metco, Westbury, NY, USA). The coatings were deposited onto Ti–6Al–4V substrates that had been grit-blasted before spraying.

Particle diagnostics were performed in order to evaluate in-flight particle properties. For this purpose, an in-flight diagnostic tool (DPV 2000, Tecnar Automation, Saint Bruno, QC, Canada) was employed. This system uses infrared pyrometry in order to perform the in-flight diagnostics on 5000 sprayed particles.

Different propylene flow rates were tested by monitoring particle temperature and velocity. The parameter sets selected for coating production were the ones that produced similar values for average particle temperature ($\sim 30^\circ\text{C}$ above the melting point of titania) and velocity in the thermal spray jet for the three different feedstock powders. The measurements were performed

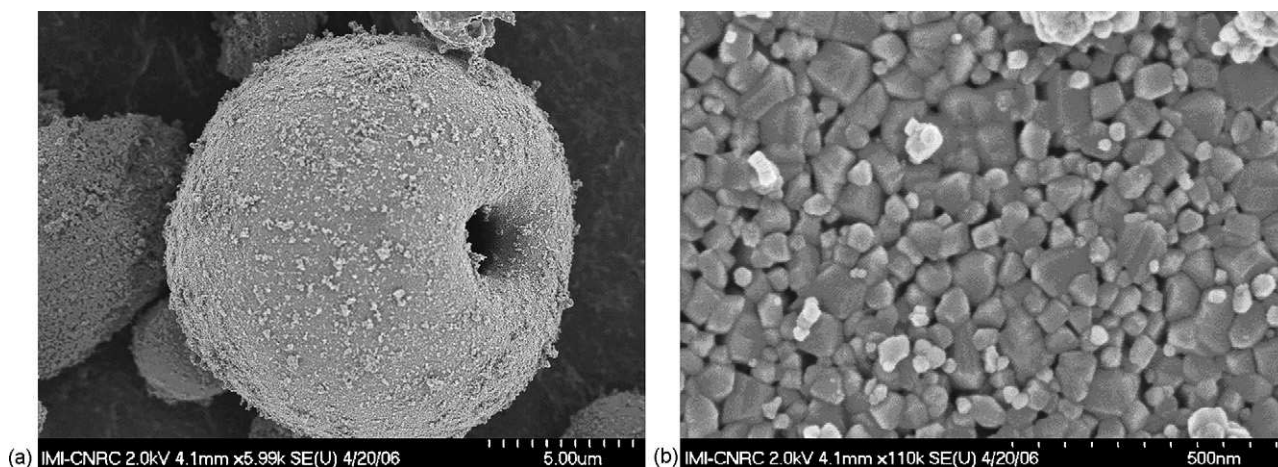


Fig. 1. (a) Morphology of spray-dried titania feedstock particle. (b) Particle of (a) observed at higher magnification—individual nanosized titania particles.

from the centerline of the HVOF jet at the standoff distance for coating deposition (20 cm).

Moreover, during the spraying process the substrate temperature was recorded using a pyrometer. In order to reduce the coating temperature, a cooling system (air-jets) was used and the temperature was kept below 170 °C for all the coatings.

2.3. Structure and phase characterization

Powder morphology, surface topography and cross-sections of the coatings were examined using field emission scanning electron microscopy (FE-SEM). Samples were cut with a diamond saw, vacuum impregnated with a low viscosity epoxy resin (Caldo Fix, Struers, USA) and, finally, polished using standard metallographic procedures. Ten images of the cross-section of each coating were analyzed via image analysis in order to determine the porosity levels.

The phases present in both the starting powder and the coatings were determined by means of X-ray diffraction (XRD) using Cu K α radiation and a scan speed of 0.05° for values of 2θ between 20° and 60°.

Roughness and surface topography are important parameters in biocompatible coatings [16,17]. Roughness measurements of the HVOF coatings were carried out by two different techniques: (i) tactile roughness tester (profilometer Mitutoyo SurfTest 301, Mitutoyo, Japan) and (ii) confocal microscopy, which is a non-contact optical imaging profiler (PLu 2300 Optical Profiler, Sensofar-Tech, SL, Barcelona, Spain). In the latter case, roughness profiles were obtained by filtering the roughness effects for which the wavelength was superior to the selected cut-off length (λ_c). A cut-off value of 0.800 mm was selected, using a filter of Gaussian type as recommended by the norm ISO 11562:1996 [18]. For each technique, 10 measurements were carried out at various positions on the surface, then the coefficient of variance, the average and the standard deviation were calculated.

2.4. Mechanical properties

Vickers microhardness measurements (Micromet II, Buehler, Lake Bluff, IL, USA) were performed under a 300 g load for

15 s on the polished cross-section of the coatings. A total of 30 microhardness measurements were carried out for each coating in order to achieve a constant value of coefficient of variance (CV). It was necessary to adopt this procedure to ensure that there were enough statistical data to determine with precision the Weibull modulus distribution of the hardness values for each coating [19].

The bond strength of the coatings was tested using the ASTM standard C633-01 for determining the adhesion or cohesion strength of thermal spray coatings [20]. A total of five samples of each coating were employed, and the bond strength data was reported as the average value.

3. Results and discussion

3.1. Feedstock and particle size distribution

Fig. 1(a) shows the morphology of the nanostructured titania powders that were used in this work. It can be observed that the morphology of the spray dried titania feedstock was predominantly spherical, exhibiting the typical donut shape of spray dried particles. When analyzed at high magnification (Fig. 1b) it is possible to observe an agglomeration of titania nanoparticles smaller than 100 nm, indicating that the titania feedstock is nanostructured. The HA powder was also spray dried resulting in spherical particles (Fig. 2a). After the process of spray drying, the powders were sintered and densified (Fig. 2b) by the manufacturer. It can be observed that the internal structure of the HA particles is somewhat coarser than that of the TiO₂ particles.

Powder particle blends were observed after the mechanical mixing step. Fig. 3 shows a micrograph and the mapping spectra for the elements calcium and titanium in the nanostructured TiO₂ + 20 wt% HA powder system. It may be noted that the two constituents are relatively uniformly distributed in the mixture. Moreover, Fig. 4 shows the size distribution of the different feedstock powders, where it can be observed that the three feedstock powders exhibited similar particle size distributions.

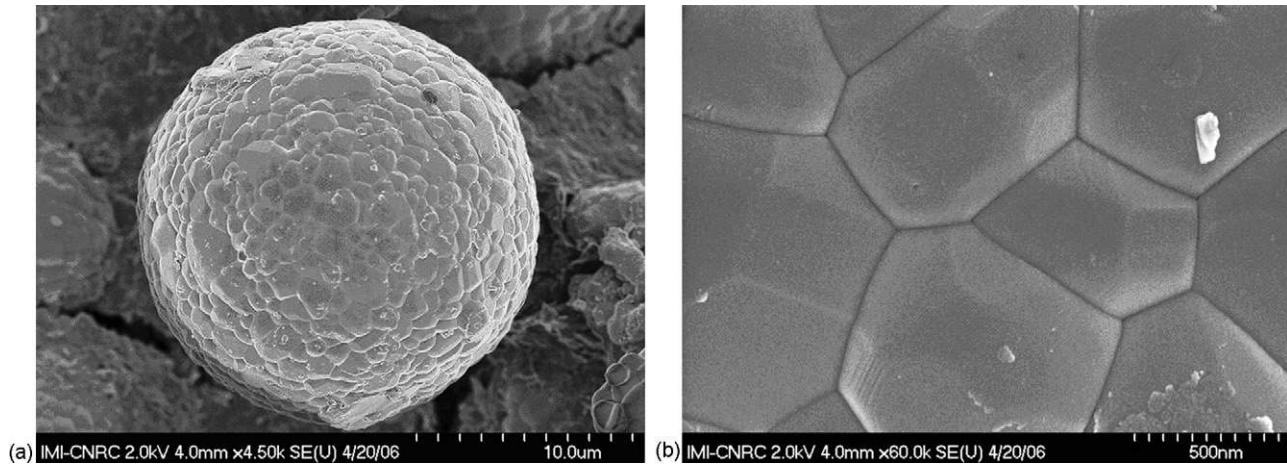


Fig. 2. (a) Morphology of spray-dried and sintered HA feedstock particle. (b) Particle of (a) observed at higher magnification—dense particle as a result of the sintering process.

3.2. In-flight particle characteristics

Fig. 5 shows the particle temperature and velocity distributions in the thermal spray jet for the three feedstock powders. The three sprayed powders showed similar distributions for the spraying parameters employed. Fig. 6 shows the histograms of particle diameter, temperature and velocity for the three spray parameters. It is possible to observe that the shapes of the distributions for the three spraying conditions are similar. The average particle temperature and velocity for the different spraying parameters are summarized in Table 1. That table shows that the average particle temperatures and velocities were in the range of 1874–1881 °C and 651–686 m/s. Therefore, the average particle temperature of all three spraying conditions was slightly above the melting point of titania (1855 °C) [21].

The thermal conductivity (K) of the titania and hydroxyapatite bulk materials are 7.4 and 1.25 W/mK, respectively [21], so titania is more able to conduct heat. Therefore more thermal energy is required for an HA particle to reach a given temperature level than needed for a TiO₂ particle. In fact, it was observed that during HVOF spraying it was necessary to use a higher propylene flow when spraying nanostructured TiO₂ + HA as compared to that required when spraying pure nanostructured TiO₂.

It is important to point out that the objective of HVOF spraying the three feedstock powders at similar levels and distributions of particle temperature and velocity was achieved. Therefore, it is assumed that the difference in results and characteristics of residual stress, microstructure, phase content and mechanical properties discussed in the next sections are mainly related to the

composition of each feedstock, and not to the in-flight particle characteristics.

3.3. Microstructural characterization of the coatings

Figs. 7–9 show the cross-section of the coatings. It is possible to observe that the nanostructured TiO₂ coating microstructure is relatively dense and homogeneous, not exhibiting the typical layered or lamellar structure of thermal spray coatings (Fig. 7). It may be assumed that this coating exhibits an isotropic “bulk-like” microstructure and low porosity (3%) due, in part, to the high particle velocity at the point of impact with the substrate (686 ± 93 m/s).

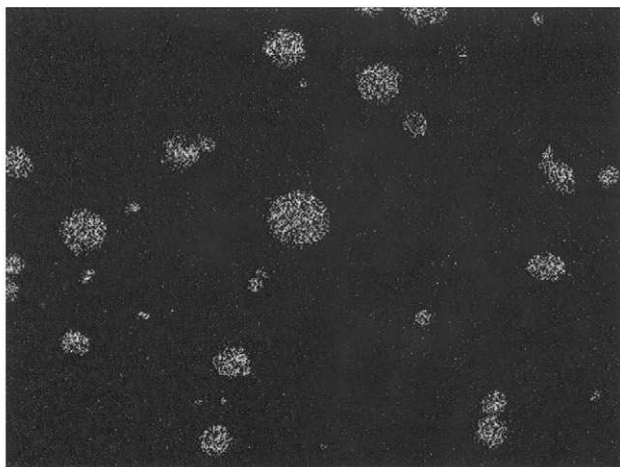
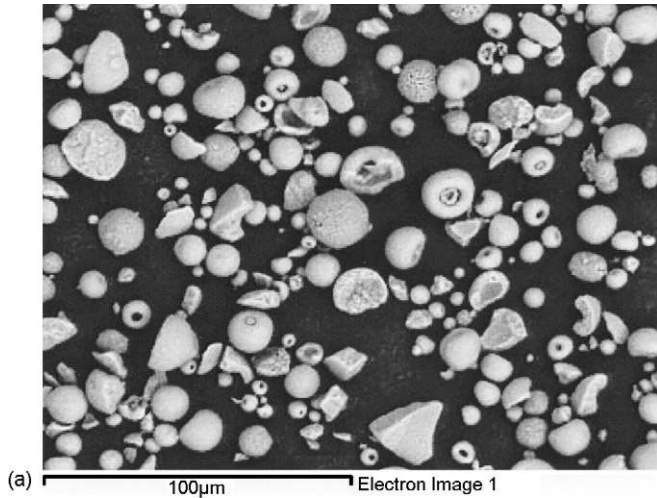
After spraying, the HA and TiO₂ phases were relatively homogeneously distributed in the coatings (Figs. 8 and 9). HA appears as lamellae in a titania matrix, but some spherical HA particles were also observed. The spherical particles represent HA particles that were slightly melted (outer shell) in the thermal spray jet. It is important to point out that HA has lower thermal diffusivity and conductivity values than those of titania. The porosity levels of the nanostructured TiO₂ + 10 wt% HA and nanostructured TiO₂ + 20 wt% HA coatings were less than 1%.

The as-sprayed top surfaces of the nanostructured TiO₂ + HA coatings are shown in Figs. 10 and 11. The surfaces were composed of titania and 20–30 μm diameter HA splats. This structure could be very interesting for biomedical applications due to the combination of the non-absorbable (stable) titania phase, and the bioactive HA phase.

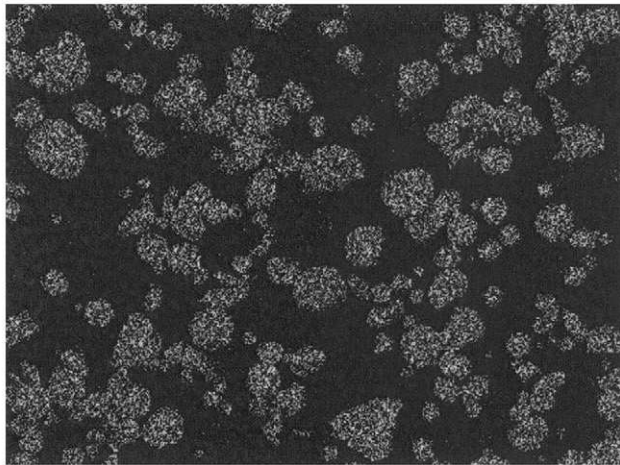
The roughness values of the HVOF sprayed coatings measured by confocal microscopy and a contact tester are shown in Fig. 12. The same trend for the results was obtained for both techniques, although the roughness values and the standard deviation acquired by means of confocal microscopy were lower than those obtained by the roughness contact tester. The results indicated some increase of roughness with the hydroxyapatite content in titania coatings. The nanostructured TiO₂ + 20 wt% HA coating exhibited the highest roughness, which suggests that the roughness may be dominated by the HA splats since the topography of the titania is partially masked.

Table 1
HVOF average particle temperature and velocity for each system

wt% HA	T (°C)	V (m/s)
0	1881 ± 162	686 ± 93
10	1875 ± 135	651 ± 88
20	1874 ± 132	654 ± 91



Ca Ka1



(b) Ti Ka1

Fig. 3. Micrograph (a) and X-ray maps (b) showing Ca and Ti for the nanostructured titania + 20 wt% HA powder.

3.4. Phase content

The XRD patterns of the as-sprayed titania coating and the nanostructured feedstock powder are shown in Fig. 13. The volume percentage of anatase was determined according to the

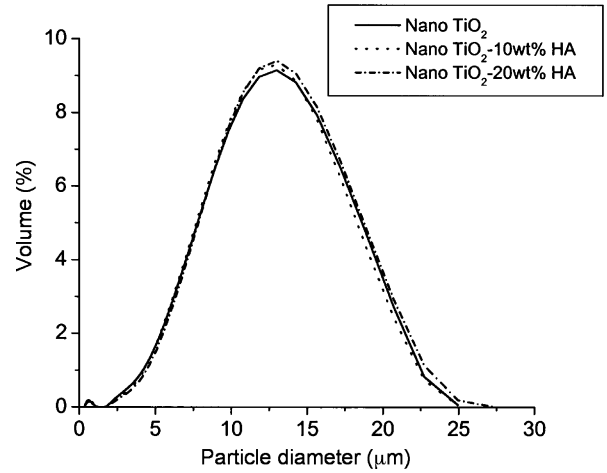


Fig. 4. Size distribution of the different powders sprayed.

following equation [22]:

$$C_A = \frac{8I_A}{(13I_R + 8I_A)} \tag{1}$$

where I_A and I_R are the X-ray intensities of the anatase (1 0 1) and the rutile (1 1 0) peaks, respectively. It can be observed that a phase transformation occurred during the thermal spraying of titania. The starting powder was mainly composed of anatase (86%); and after spraying, the amount of anatase was reduced to 17%, with the main phase being rutile. Of the three polymorphic forms of titania, rutile is the only stable phase, whereas anatase and brookite are metastable and are transformed to rutile irreversibly by heating. The anatase-rutile transition has been reported to take place between 400 and 1000 °C, depending on the microstructure of the powders of anatase, the impurity content, deviations in the stoichiometry, superficial area and particle size [21]. The residual anatase phase present in the coating was probably the result of semi-molten nanostructured powder particles that were embedded in the coating microstructure. It is important to point out that these semi-molten nanostructured particles (nanozones) present in the coating are believed to be responsible for the good mechanical performance of the coating via the enhancement of its toughness [6,7].

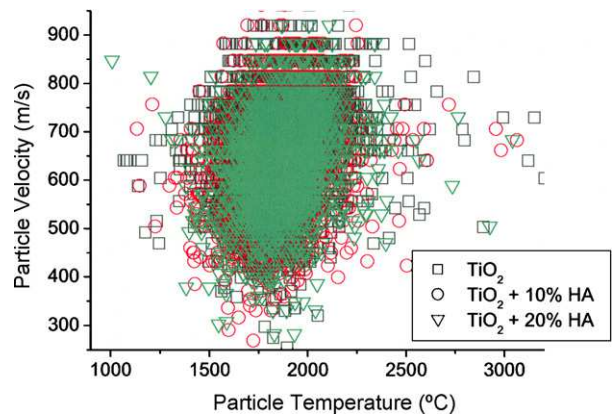


Fig. 5. Particle velocity vs. particle temperature for the three types HVOF-sprayed feedstock particles.



Fig. 6. Histograms of particle diameter, velocity and temperature for the three types of HVOF-sprayed feedstock particles.

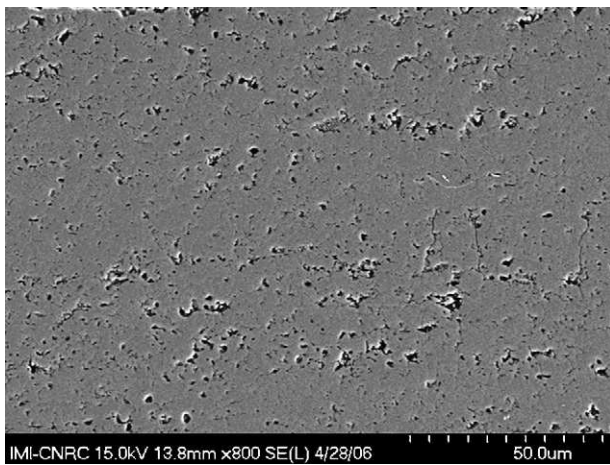


Fig. 7. Cross-section of the HVOF-sprayed nanostructured TiO_2 coating.

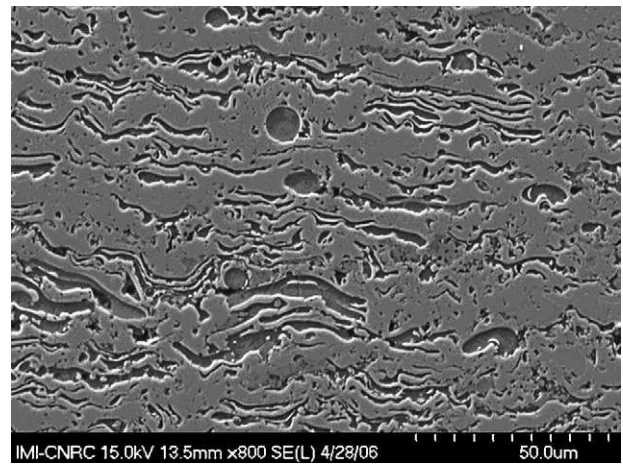


Fig. 9. Cross-section of the HVOF-sprayed nanostructured $\text{TiO}_2 + 20\% \text{ wt HA}$ coating.

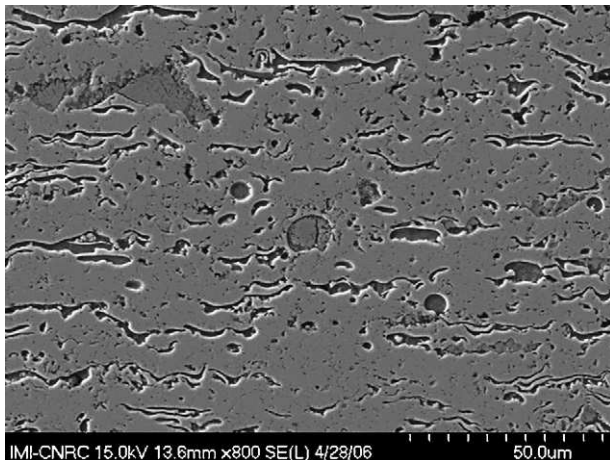


Fig. 8. Cross-section of the HVOF-sprayed nanostructured $\text{TiO}_2 + 10\% \text{ wt HA}$ coating.

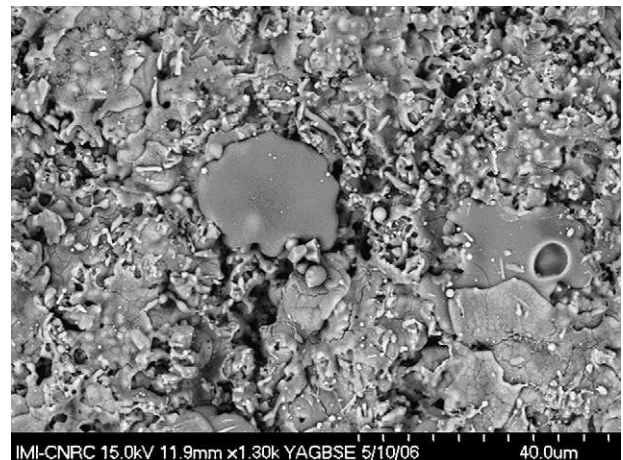


Fig. 10. As-sprayed top surface of the HVOF-sprayed nanostructured $\text{TiO}_2 + 10\% \text{ wt HA}$ coating.

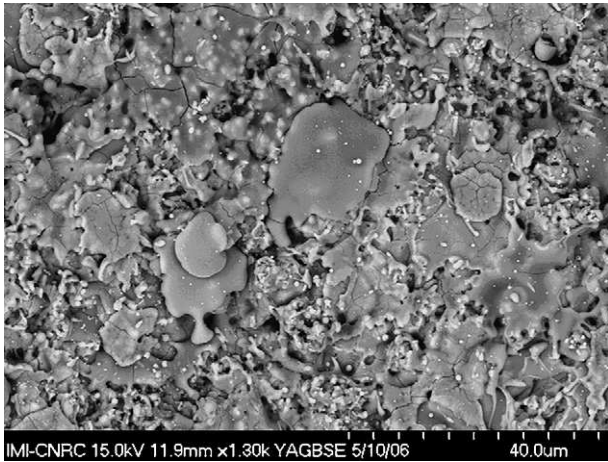


Fig. 11. As-sprayed top surface of the HVOF-sprayed nanostructured TiO₂ + 20 wt% HA coating.

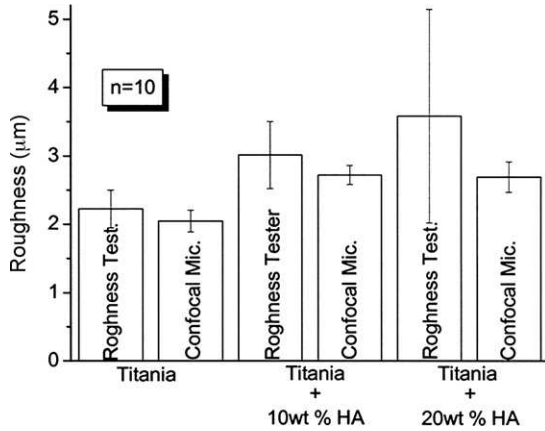


Fig. 12. Roughness values obtained for the different coatings and by two different techniques.

Figs. 14 and 15 show the patterns of the nanostructured TiO₂ + HA systems. These compositions exhibited transformations similar to the titania coating: the rutile peak intensity increased considerably after spraying, but the anatase peak intensity decreased. The feedstock powders and coatings were mainly

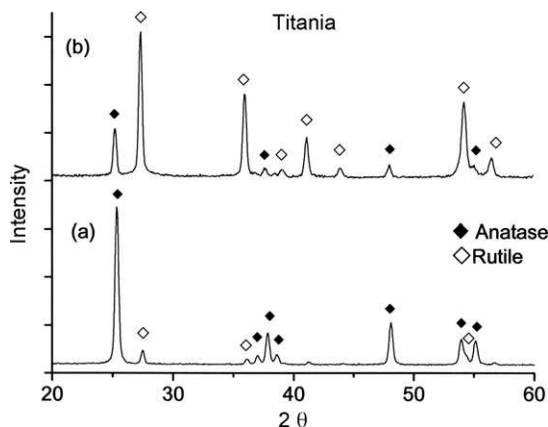


Fig. 13. XRD patterns of the nanostructured TiO₂ feedstock (a) and HVOF-sprayed coating (b).

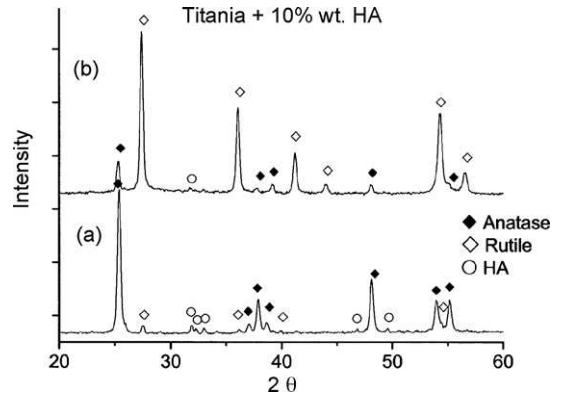


Fig. 14. XRD patterns of the nanostructured TiO₂ + 10 wt% HA feedstock (a) and HVOF-sprayed coating (b).

composed of HA (JCPDS 9-432), rutile (JCPDS 21-1276) and anatase (JCPDS 21-1272) [23]. No tricalcium, tetracalcium phosphate or CaO often produced due to the thermal decomposition of HA were detected by XRD. The reasons why other calcium phosphate phases were not detected in the coatings may be related to the fact that titania was the main phase and may have masked the XRD peaks of other calcium phosphate phases if they were formed in small amounts [24]. Moreover, no chemical products resulting from the reaction between HA and TiO₂ were observed following the spraying. The absence of such evidence in the XRD spectra was probably caused by the (i) fact the powders were blended (i.e., not intimately mixed) and (ii) short time that the particles were in the HVOF jet [25].

3.5. Hardness and Weibull modulus

Fig. 16 shows the Vickers hardness values (300 g load) obtained for the cross section of the HVOF coatings. The coefficient of variation (CV) for the hardness measurements on each sample stabilized around 20 measurements and, therefore, 30 microhardness measurements were taken for each sample. As expected, the hardness values were decreased by the addition of HA.

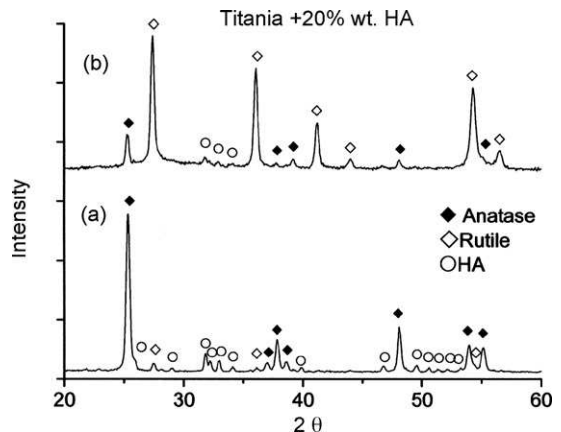


Fig. 15. XRD patterns of the nanostructured TiO₂ + 20 wt% HA feedstock (a) and HVOF-sprayed coating (b).

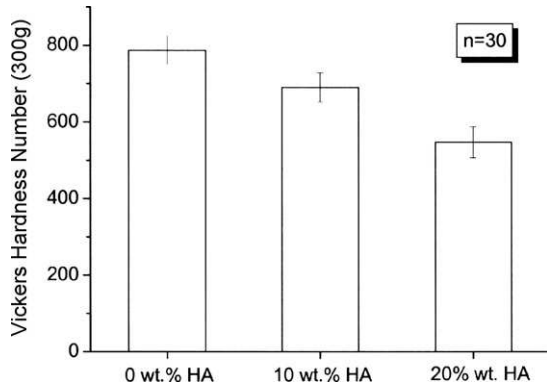


Fig. 16. Vickers hardness of the HVOF-sprayed coatings.

Fig. 17 shows the Weibull modulus distribution of the hardness on the cross-section of the three HVOF coatings. The Weibull modulus measures the variability of the mechanical properties of ceramic materials. According to Weibull theory, the cumulative probability that a sample will yield at a particular random property value (x_i) is P_i :

$$P_i = 1 - \exp \left[- \left(\frac{x_i - x_u}{x_0} \right)^m \right] \quad (2)$$

where x_0 is a normalizing constant that represents the characteristic value below which 63.2% of the data lie, x_u the threshold value below which there is no failure, and m is the Weibull modulus which defines the shape of the distribution.

A more useful determination of the Weibull modulus is to estimate the probability of yield at a particular value for each sample as $P_i = i/(N + 1)$. One first ranks the samples in order of increasing mechanical property value and assigns an index $i = 1$ for the lowest value x_1 , $i = 2$ for the second lowest value x_2 , and so on, up to $i = N$ for the highest value of mechanical property x_N . Then the data is finally plotted in the following linearized form of the Weibull distribution:

$$\ln \left[\ln \left(\frac{1}{1 - P_i} \right) \right] = m \ln x_u - m \ln x_0 \quad (3)$$

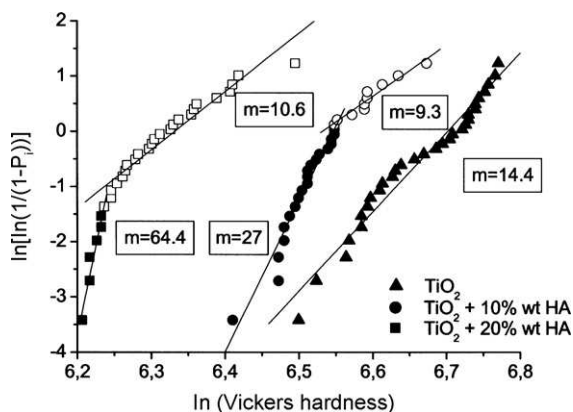


Fig. 17. Weibull modulus distributions of the Vickers hardness of the HVOF-sprayed nanostructured TiO₂ and the two nanostructured TiO₂ + HA coatings.

Table 2

Weibull modulus values of the Vickers hardness of the HVOF-sprayed coatings

System (wt% HA)	Weibull modulus
0	14.4
10	9.3
20	10.6

where Weibull modulus, m , is the slope of the $\ln[\ln(1/(1 - P_i))]$ versus $\ln x_u$ plot [26]. The values of the Weibull modulus are summarized in Table 2.

The Vickers hardness Weibull plot of the titania coating exhibits a linear behaviour indicative of the homogenous coating structure (Fig. 17). A Weibull modulus of 14.4 was found for this coating. However, the Weibull modulus plots of the titania-HA coatings exhibit a bimodal distribution. In order to determine the exact point where the slopes of the bimodal coatings (nanostructured TiO₂ + 10 wt% HA and nanostructured TiO₂ + 20 wt% HA) are localized in Fig. 17, the r^2 statistics were determined with respect to the number of measurements. The r^2 factor was plotted for 3, 4, 5, etc. measurements of $\ln[\ln(1/(1 - P))]$ until all the 30 measurements were taken into account. For each one of the bimodal coatings, there was a point where the r^2 maximum was achieved (peak). This data value corresponds to a transition point between the two distributions [27]. It should be pointed out that the Vickers hardness impressions in the nanostructured TiO₂ + HA coatings exhibited diagonal lengths on the order of 25–35 μm . As thermally sprayed splats normally exhibit thicknesses around 1 μm or of just a few microns, and by observing the scale of features in the coating microstructures (Figs. 8 and 9), it can be assumed that each indentation sampled both nanostructured TiO₂ and HA phases at the same time, i.e., individual phases (regions) of TiO₂ and HA were probably not sampled. However, probably there were regions in the microstructure of the coatings where the TiO₂-HA mixture was more homogeneous than others. Therefore, the regions exhibiting higher homogeneity would probably present higher Weibull modulus values (less data scattering) than those regions with lower degree of TiO₂-HA homogeneity, thereby giving rise to the bimodal distribution. It is important to point out that for the bimodal coatings, the upper slope of the Weibull moduli distributions exhibit a similar value (~ 9 to 11). It is also observed that as the HA content increases from 10 to 20%, the length of the upper slope increases and the lower slope tends to be minimized. From this observation, it can be inferred that if the HA content is increased to values higher than 20 wt%, the bimodal distribution will probably tend to disappear. This would occur because the degree of mixing of both phases (TiO₂ and HA) would become more uniform for higher amounts of HA. The distribution of both phases would tend to become so homogeneous, that a linear distribution would be observed.

3.6. Bond strength

Nanostructured titania and nanostructured TiO₂ + 10 wt% HA coatings failed at the epoxy glue during bond strength testing (ASTM C633). Because these samples had a glue failure, the

exact bond strength of these thermal spray coatings could not be quantified. The strength of the epoxy glue was previously tested and indicated a value of 77 MPa ($\sim 11,000$ psi), therefore, the bond strength of the nanostructured titania and nanostructured $\text{TiO}_2 + 10$ wt% HA coatings was higher than this value. However, the nanostructured $\text{TiO}_2 + 20$ wt% HA coatings showed an adhesive-cohesive failure and an adhesion value of 68 ± 14 MPa, which demonstrates that the addition of HA weakened the bond strength of the HVOF-sprayed nanostructured titania coating. This lower value could be attributed to the weak mechanical bonding between HA and titania splats, where apparently no chemical reaction occurred, and to the known low mechanical performance of HA. It is important to point out that this value (68 ± 14 MPa) is higher than those generally found in the literature for thermal spray HA coatings (e.g., 31 MPa) [28] or HVOF-sprayed conventional $\text{TiO}_2 + \text{HA}$ coatings (e.g., 28 MPa) [24].

4. Conclusions

In this work, nanostructured TiO_2 , nanostructured $\text{TiO}_2 + 10$ wt% HA and nanostructured $\text{TiO}_2 + 20$ wt% HA were HVOF sprayed with powders having similar particle size distributions and similar distributions of the in-flight particle characteristics (i.e., temperature and velocity). Because of this approach, it is believed that differences of microstructure and properties of the engineered coatings observed in this work were mainly related to the powder morphology and composition, rather than to the differences in particle temperature and velocity. The majority of the anatase phase of nanostructured TiO_2 powder transformed to rutile during HVOF spraying. The anatase phase observed in the coatings was probably the result of semi-molten nanostructured TiO_2 particles embedded in the coating microstructure. For the coatings produced from the mixture of nanostructured $\text{TiO}_2 + \text{HA}$ powders, it was observed that (i) the phases were relatively homogeneously distributed in the coating microstructure and (ii) no significant chemical reaction occurred between the two constituents (TiO_2 and HA) of the sprayed powders. In addition, no significant HA degradation was observed by means of XRD. The Vickers hardness results and the adhesion tests showed that the addition of HA weakened the mechanical properties of the titania coatings, however, the bond strength values obtained were higher than those generally found in the literature for thermally sprayed HA coatings. The nanostructured $\text{TiO}_2 + \text{HA}$ coatings tended to exhibit the highest values of roughness, which suggests that the roughness may be dominated by the HA splats since the topography of the titania tends to be masked by the HA particles. As HA is a bioactive material, this surface characteristic found in this study is probably very interesting for biomedical applications. A bimodal Weibull distribution was observed for the hardness values of the nanostructured titania + HA coatings. This bimodal distribution tends to disappear as the HA content increases, as an indicator of the homogeneity of the phase distribution, i.e., the two phases tend to be well-distributed throughout the coating microstructure. The HVOF-sprayed nanostructured titania + HA coatings

may become a very interesting alternative for biomedical applications due to the combination of a high mechanical performance and non-absorbable nanostructured TiO_2 phase (stable), and a bioactive HA phase, that can enhance the bio-performance of the coating.

Acknowledgements

The authors thank J.-F. Alarie for metallography and adhesion testing, F. Belval for HVOF spraying, M. Lamontagne for in-flight particle diagnostics and M. Thibodeau for SEM observations. Moreover, M. Gaona thanks the Generalitat de Catalunya (Spain) for the Formació de Personal Investigador (FI) grant and the Thermal Spray Centre for the financial support.

References

- [1] P. Cheang, K.A. Khor, *Biomaterials* 17 (1996) 537–544.
- [2] L. Sun, C.C. Berndt, C.P. Grey, *Mater. Sci. Eng. A* 360 (2003) 70–84.
- [3] M.T. Manley, W.N. Capello, J.A. D'Antonio, A.A. Edidin, R.G.T. Geesink, *J. Bone Joint Surg.* 80A (1998) 1175–1185.
- [4] O. Reikeras, R.B. Gunderson, *Acta Orthop. Scand.* 73 (2002) 104–108.
- [5] K.A. Gross, W. Walsh, E. Swarts, *J. Therm. Spray Technol.* 13 (2004) 190–197.
- [6] R.S. Lima, B.R. Marple, *Mater. Sci. Eng. A* 395 (2005) 269–280.
- [7] R.S. Lima, B.R. Marple, *Surf. Coat. Technol.* 200 (2006) 3428–3437.
- [8] J. Shi, C. Ding, Y. Wu, *Surf. Coat. Technol.* 137 (2001) 97–103.
- [9] J.-G. Legoux, F. Chellat, R.S. Lima, H. Shen, B.R. Marple, M.N. Bureau, G.A. Candelieri, *J. Therm. Spray Technol.*, in press.
- [10] L.G. Gutwein, T.J. Webster, *Biomaterials* 25 (2004) 4175–4183.
- [11] T.J. Webster, C. Ergun, R.H. Doremus, R.W. Siegel, R. Bizios, *J. Biomed. Mater. Res.* 51 (2000) 475–483.
- [12] R. Rohanzadeh, M. Al-Sadeq, R.Z. LeGeros, *J. Biomed. Mater. Res.* 71 (2004) 343–352.
- [13] R.S. Lima, H. Li, K.A. Khor, B.R. Marple, *J. Therm. Spray Technol.*, in press.
- [14] J. Li, *Biomaterials* 14 (3) (1993) 229–232.
- [15] P.A. Ramires, A. Romito, F. Cosentino, E. Milella, *Biomaterials* 22 (2001) 1467–1474.
- [16] G. Lauer, M. Wiedmann-Al-Ahmad, J.E. Otten, U. Hübner, R. Schmelzeisen, W. Schilli, *Biomaterials* 22 (2001) 2799–2809.
- [17] K. Cai, J. Bossert, K.D. Jandt, *Colloids Surf. B: Biointerfaces* 49 (2006) 136–144.
- [18] Geometrical Product Specifications (GPS), Surface texture: profile method—metrological characteristics of phase correct filters. Standard ISO 11562:1996 -International Organization for Standardization.
- [19] C.K. Lin, C.C. Lin, C.C. Berndt, *J. Am. Ceram. Soc.* 78 (1995) 1406–1410.
- [20] Standard Test Method for Adhesion or Cohesion of Thermal Spray Coatings, ASTM Standard C 633-01. ASTM, West Conshohocken, PA, USA.
- [21] M. Miyayama, K. Koumoto, H. Yanagida, *Engineering properties of single oxides*, in: S.J. Schneider (Ed.), *Engineered materials handbook, 4-ceramic and glasses*, ASM International, Materials Park, OH, 1991, pp. 748–757.
- [22] N. Berger-Keller, G. Bertrand, C. Filiatre, C. Meunier, C. Coddet, *Surf. Coat. Technol.* 168 (2003) 281–290.
- [23] Powder Diffraction File Alphabetic PDF-2 Data Base, file 9-432, 21-1276 and 21-1272. International center of diffraction Data, Newton Square, PA, USA, 1994.
- [24] H. Li, K.A. Khor, P. Cheang, *Biomaterials* 23 (2002) 85–91.
- [25] J. Weng, X. Liu, X. Zhang, X. Ji, *J. Mater. Sci. Lett.* 13 (1994) 159–161.
- [26] R.S. Lima, B.R. Marple, *J. Therm. Spray Technol.* 12 (2003) 360–369.
- [27] R.S. Lima, A. Kucuk, C.C. Berndt, *Mater. Sci. Eng. A* 327 (2002) 224–232.
- [28] H. Li, K.A. Khor, P. Cheang, *Mater. Sci. Eng. A* 293 (2000) 71–80.